Journal of Solid State Chemistry **148,** 178–185 (1999)
Article ID jssc.1999.8486, available online at http://www.idealibrary.com on IDEAL®

Following the Formation of γ-Phase Bi_2MoO_6 Catalyst by *in Situ* XRD/XAS and Thermogravimetric Techniques

L. M. Reilly, G. Sankar, and C. R. A. Catlow

Davy Faraday Research Laboratory, The Royal Institution of Great Britain, 21 Albemarle Street, London W1X 4BS, United Kingdom

Received May 27, 1999; in revised form July 28, 1999; accepted August 11, 1999

We report a detailed *in situ* study of the preparation of the γ-phase Bi_2MoO_6 catalyst from a gel. In particular, the local coordination around molybdenum remained tetrahedral, although the poorly crystalline bismuth molybdate phase started to appear below 400°C; above this temperature there was a distinct change in the coordination around molybdenum to a distorted octahedron. Combining the information obtained from TGA, DTA, combined XRD/XAS and DRIFT techniques, we were able to track clearly the changes in the local coordination around the molybdenum as well as the loss of water and ammonia molecules during the course of the formation of the crystalline γ-Bi_2MoO_6 phase from a poorly crystalline material. © 1999 Academic Press

INTRODUCTION

Bismuth molybdates have the general chemical formula $Bi_2O_3 \cdot nMoO_3$, where $n = 3, 2$, or 1, corresponding to the α, β, and γ phases, respectively. They are known to be good catalysts for the selective oxidation or ammoxidation of lower olefins (1–3). The three phases have been studied extensively to understand the relationship between structure and catalytic properties (4); indeed, all the three phases are shown to be efficient catalysts. The structures of the α and β phases can be considered as defective fluorite structures, whereas the γ phase is an Aurivillius type structure (4–6). In addition to this structural difference, the local coordination around molybdenum is tetrahedral in both the α and β phases and distorted octahedral in the γ phase (7). The γ phase is of particular interest, since this material is not only a good catalyst, but also shows an unusual phase transformation above 600°C to the γ'' phase which further transforms to the γ' phase (8). The first phase change is reversible. The second is irreversible. Although the complete structure of the γ'' phase is yet to be solved, in a recent publication (8) it was shown that the distorted MoO_6 octahedron undergoes further elongation of the two long Mo–O bonds before transforming to a tetrahedral coordination. Several techniques, especially diffraction methods and high-resolution electron microscopy have been employed to elucidate the structure of all these phases (4–7). However, the production of the final phase, i.e., the active catalyst, is poorly understood. Here we report a detailed characterization carried out during the synthesis of Bi_2MoO_6 system from a precursor-gel, using a suite of *in situ* methods.

The techniques used are the conventional TGA, DSC methods, and combined X-ray diffraction/spectroscopy (XRD/XAS) which is ideal for deriving information about both long-range ordering (phase formation) as well as local structural changes around a specific metal ions (9, 10). This latter technique is now widely employed in the study of a variety of solid state systems, which include catalysts (11, 12), nanomaterials (13), and phase transformations in ceramics, glasses, and zeolites (14, 15). In addition, we have used diffuse-reflectance infrared spectroscopy to complement the results obtained from the other techniques. Our investigation clearly showed that during the phase formation there are significant alterations in the coordination around molybdenum whereas the bismuth environment remains nearly unchanged.

EXPERIMENTAL

The precursor gel was prepared following the standard procedure (8). Appropriate amounts of ammonium heptamolybdate were dissolved in ammonium hydroxide. This solution was mixed with a bismuth nitrate solution. The pH of the resulting solution was adjusted to ca. 6.5 by adding ammonium hydroxide. A pale yellow precipitate was formed, which is then filtered and dried at 100°C; it is then used as the starting material for further studies.

Both DSC and TGA measurements were carried out using Shimadzu instruments. The samples were heated in air and the data were recorded in the temperature range 25 to 450°C.

Combined XRD/XAS (9) data were collected at station 9.3 of Daresbury Laboratory (which operates at 2 GeV with typical currents in the range 150 to 250 mA). This station is

0022-4596/99 $30.00
Copyright © 1999 by Academic Press
All rights of reproduction in any form reserved.

equipped with a Si(220) monochromator and ion chambers for measuring incident (I_0), transmitted (I_t) beam intensities and an INEL position sensitive detector for collecting diffraction patterns. In a typical experiment, a self-supporting wafer containing ca. 30 mg of the sample was placed in the *in situ* cell. This sample was heated in air from room temperature to 400°C at 5°C min^{-1} and held there for 60 min before heating further to 530°C (at 5°C min^{-1}) and held at this temperature for 120 min. XRD and XAS data were collected sequentially during the course of heating the sample. XRD data were collected at a wavelength of 0.6272 Å, which is well below the Mo*K*-edge, in order to avoid fluorescence effects. XRD and Mo*K*-edge data were collected for 180 and 380 s, respectively, thus resulting in a total cycle time of 10 min, which includes dead time of 40 s. The NBS silicon standard was used to calibrate the INEL detector and molybdenum foil was used to calibrate the position of the Mo*K*-edge.

XAS data were processed using the suite of programs available at the Daresbury Laboratory, namely EXCALIB (for converting the raw data to energy vs absorption coefficient), EXBROOK (for pre-edge and post-edge background subtraction) and EXCURV92 for the detailed analysis to extract structural information. The raw EXAFS data were used to extract structural information without Fourier filtering.

In situ diffuse reflectance Infra red spectra were collected using a Perkin–Elmer 1725X spectrometer. The sample was packed into a small silica crucible and then heated in air from room temperature to 300°C; spectra were recorded over a range of temperatures.

RESULTS

First we discuss the results of the TGA and DSC measurements, subsequently the IR results and finally the combined XRD/XAS studies.

TGA and DSC studies. Figure 1 shows the TGA plot for the γ-phase precursor heated in air. It is clear from the data that there are two distinct weight losses: a minor one occurring at temperatures of ca. 60°C (see the inset for clarity) and a major one at ca. 260°C. In Fig. 2 we show the DSC trace recorded during the heating of the sample in air. In this case we observe four distinct exothermic features occurring at 60, 131, 171, and 250°C. In addition there appears to be a small endothermic reaction between 300 and 450°C.

DRIFT measurements. IR data were collected at various temperatures using the diffuse reflectance mode, since with our present *in situ* setup it is possible to obtain IR data, at a specific temperature, only with this method rather than the transmission mode. Figure 3 shows the scans recorded at room temperature, 100, and 300°C. The most interesting changes appear in the OH and NH stretching region ca.

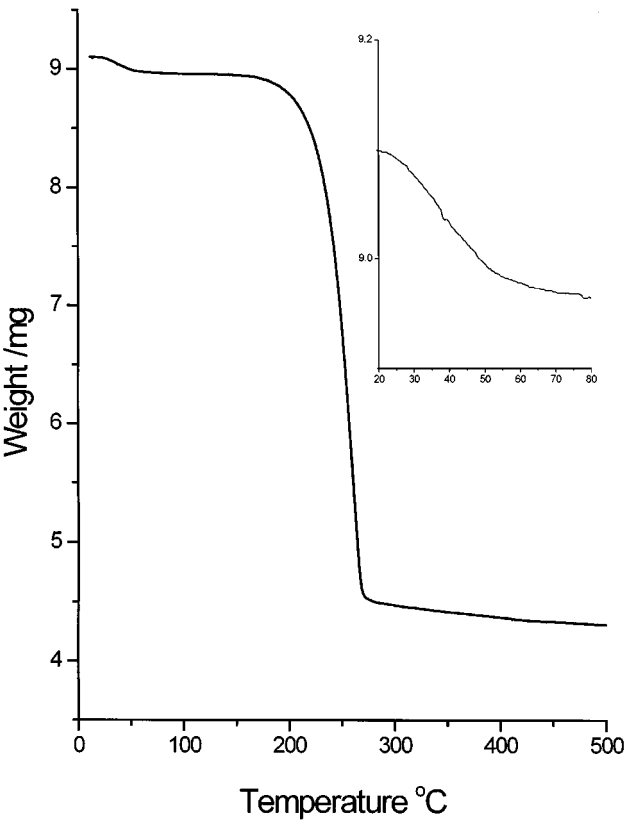

FIG. 1. TGA trace recorded during the course of heating the precursor gel of Bi_2MoO_6 in air.

3500–2500 cm^{-1}. The spectrum recorded at room temperature shows bands associated with surface H_2O molecules are clearly lost during the heating process to 100°C (the shoulder around 3500 cm^{-1} has disappeared at ca. 100°C). However, there are other OH and NH species present at this temperature. Heating to higher temperatures (above 300°C) indeed shows the clear loss of the majority of the OH and NH species. This result is consistent with DSC and TGA data.

XRD/XAS. Selected XRD patterns recorded at 50, 300, 400, and 530°C are shown in Fig. 4a. The diffraction pattern of the starting material shows a few broad peaks and upon heating these become distinct sharp reflections. The intensities of these reflections remained unaltered when the temperature was held at 400°C. On raising the temperature further, there was an increase in the intensities of all the reflections. Although it is possible to see the reflections in the XRD pattern recorded *in situ*, the quality of the data, in particular the signal to noise, is not completely satisfactory. In addition, due to the choice of wavelength as well as the experimental arrangement, it was possible to record only part of the most intense reflection of the Bi_2MoO_6 phase. In order to confirm that the observed features are not due to

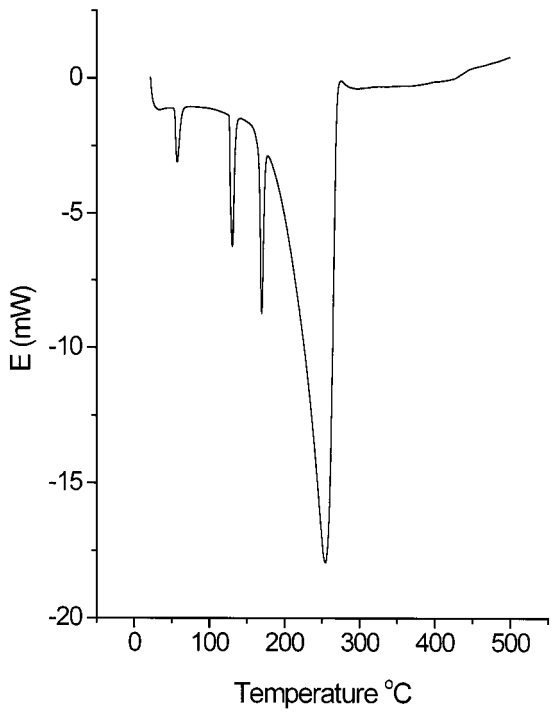

FIG. 2. DSC trace recorded during the course of heating the precursor gel of Bi_2MoO_6 in air.

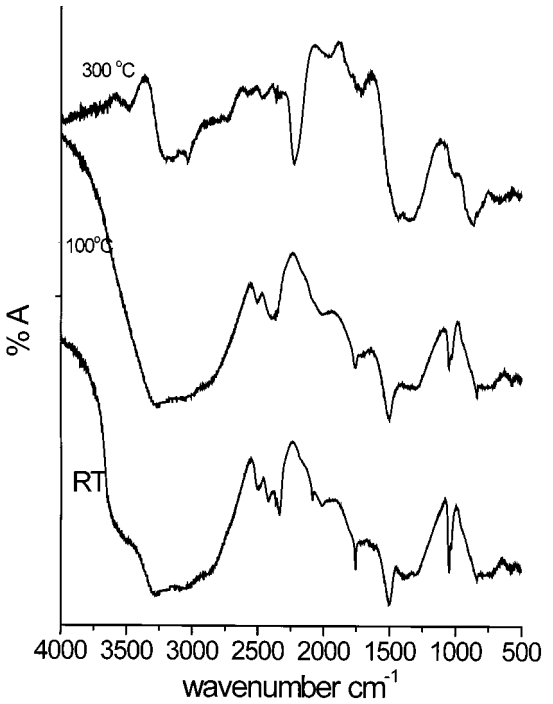

FIG. 3. FTIR spectra of Bi_2MoO_6 precursor gel recorded at various temperatures during the heat-treatment process in air.

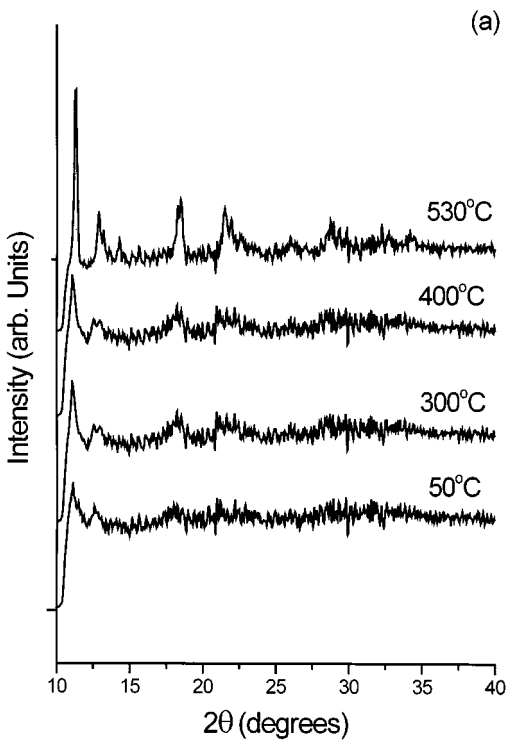

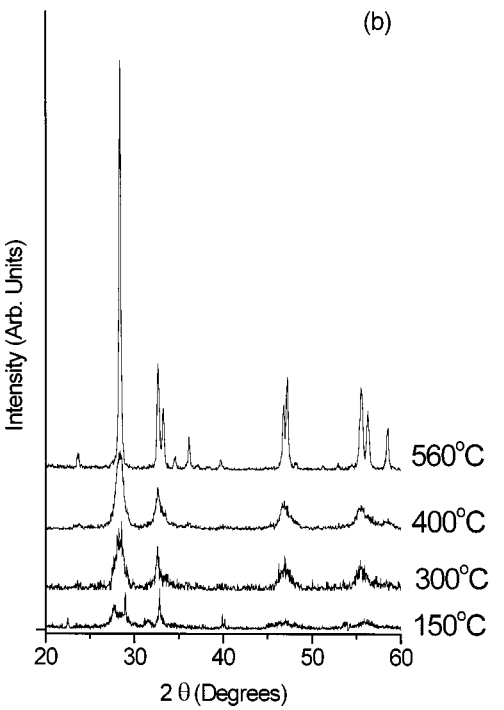

FIG. 4. (a) Selected XRD patterns recorded at 50, 300, 400, and 530°C are shown here to highlight the formation of the crystalline material. In (b) we show the XRD patterns collected using the laboratory diffractometer for the samples heated at similar temperatures as that in (a) and cooled to room temperature prior to the measurements. Note that the *in situ* measurements were performed at a wavelength of 0.6272 Å and the *ex situ* ones using Cu$K\alpha$ radiation.

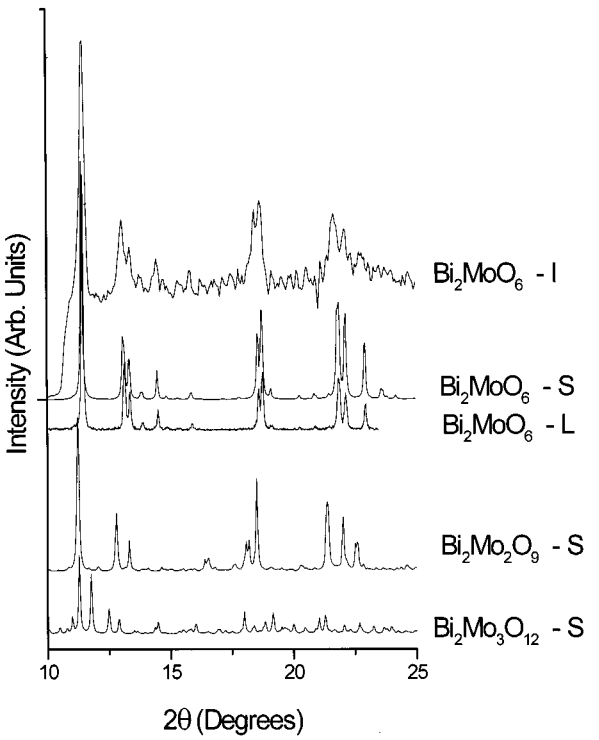

FIG. 5. XRD patterns of the three common bismuth molybdate phases, simulated using the data obtained from ICSD data base. The simulation was performed using Powder Cell software. In the simulation we have used the wavelength and step size identical to that of the *in situ* measurements and default FWHM for the peaks. All the simulated data were labelled as "S" after the compound name. "L" and "I" denotes the data corresponding to the one prepared in the laboratory and during the *in situ* studies, respectively. The data collected in the laboratory is also converted to the wavelength of 0.6272 Å to facilitate the comparison.

any artefact, we performed an identical heating procedure *ex situ*, and recorded XRD patterns for the sample at similar temperatures as in the *in situ* study; these are shown in Fig. 4b. (Note that the *in situ* data, shown in Fig. 4a were collected at a wavelength of 0.6272 Å and the XRD patterns shown in Fig. 4b were collected using the Cu$K\alpha$ radiation). Furthermore, it is clear from Fig. 5, wherein we show both the simulated XRD patterns (16) of the three most common bismuth molybdate phases along with the XRD pattern of the sample prepared in the laboratory, using well-established procedures (2, 3), and the data collected *in situ*, that the phase formed under the *in situ* conditions employed in this work is the gamma phase.

XAS scans, consisting of the near-edge region (XANES) and the post edge region (EXAFS) were analyzed independently. Mo*K*-edge XANES has a well-defined edge structure depending on its coordination geometry. Figure 6 shows a Mo*K*-edge XANES of two model compounds, MoO_3 and Na_2MoO_4 representing the octahedral and tetrahedral coordination geometry around molybdenum, respectively. MoO_3 has a distorted octahedral coordination with two Mo–O distances in the ranges of ca. 1.70, 1.94, and 2.28 Å. Na_2MoO_4 has four Mo–O distances in the region of 1.76 Å. The key features of the XANES of these two model systems are the distinct shoulders, marked as A and B in Fig. 6, characteristic for tetrahedral and octahedral coordination geometry; feature A dominates the spectra of tetrahedrally coordinated systems and B for that of the octahedrally coordinated materials. These features have been used previously (see Ref. (7) for a detailed discussion) to derive the local structure around molybdenum in many solid state and biological systems (see Ref. (17) and the references therein). Therefore the intensity of these two features can be used to estimate, qualitatively, the change in coordination geometry around molybdenum during the course of heating the precursor to form the γ-phase. Figure 7a, shows the stacked plot of the normalized-XANES data as a function temperature and in Fig. 7b we show the plot of the intensities of A and B also as a function of temperature; we note that the intensities were not obtained by fitting the data, but measuring directly the maximum value, since all the data sets were normalized with respect to the edge jump. There is a slight increase in the value of A and decrease in B up to 350°C and above this temperature a sharp decrease in A and increase in B is clearly seen in Fig. 7b. These changes in the XANES data suggest that the oxygen coordination around Mo has transformed from tetrahedral to octahedral, which will be discussed later in more detail.

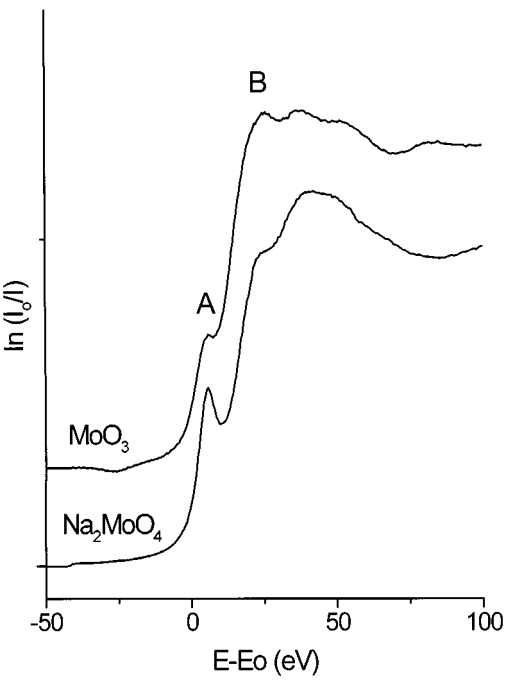

FIG. 6. Mo*K*-edge XANES plots of the two model compound MoO_3 and Na_2MoO_4. These two materials represent a typical distorted octahedral and tetrahedral coordination around molybdenum, respectively.

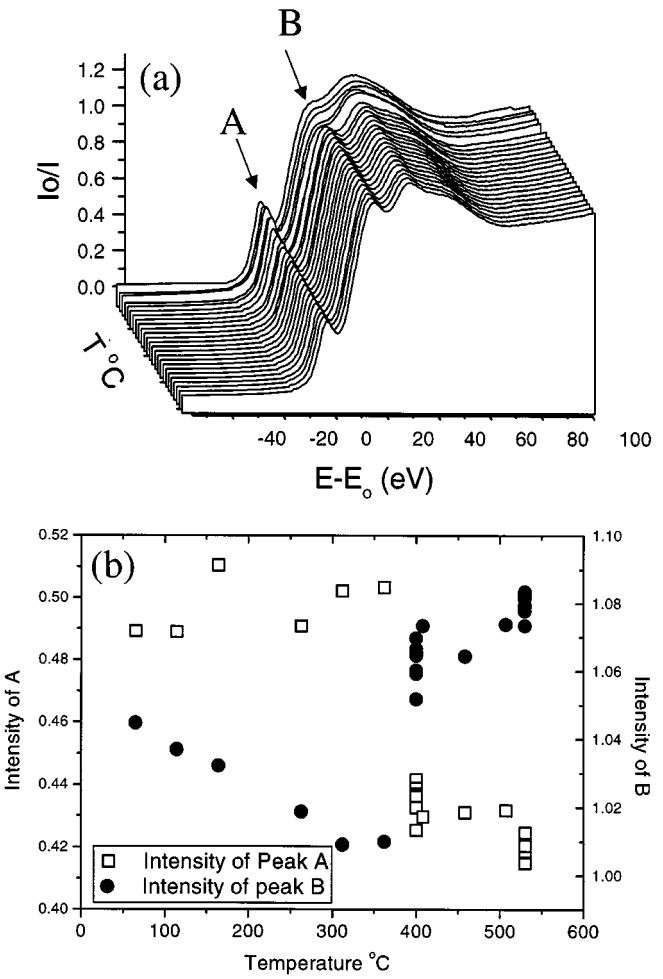

FIG. 7. (a) Stacked Mo*K*-edge XANES (obtained after normalization) plot recorded during the heat treatment of the Bi_2MoO_6 precursor gel, in air, employing the combined XRD/XAS technique. (b) Variation in the intensity of the features marked A and B in Fig. 6 as a function of temperature.

A detailed analysis of the Mo*K*-edge EXAFS was carried out to extract the structural information associated with the change in coordination geometry observed in the XANES. A stacked plot of the Fourier transforms of the EXAFS data recorded at various temperatures is shown in Fig. 8. Although minor changes in the magnitude and position of the main peak can be seen in Fig. 8, quantitative information is obtained by analyzing the EXAFS data. The change from tetrahedral to distorted octahedral coordination, implied in the XANES data, complicates the analysis of the EXAFS data, since the refinement of coordination number and Debye–Waller factor (σ^2) will produce unphysical results due to correlation effects. To overcome this problem, we used the procedure detailed in our earlier work (8), based on a distorted octahedral model to fit all the data sets. For this purpose we analyzed the data by using a starting model containing four short Mo–O distances at ca. 1.80 Å (referred as first shell) and two long Mo–O distances at ca. 2.2 Å (referred as second shell). In the refinement we allowed the Mo–O distances and their respective σ^2 to vary and held the coordination numbers constant. Thus, for example, for a tetrahedral geometry the σ^2 for the long bond at ca. 2.2 Å will be very high thereby suppressing its contribution to the EXAFS. In Fig. 8b we have plotted the $2\sigma^2$, obtained using the above-mentioned procedure for the short and long Mo–O distances, as a function of temperature. It can be seen that the σ^2 for the first shell increases only slowly with temperature, which is expected due to the increase in the temperature factor. The σ^2 for the second-shell was found to be very high (0.08) for the data sets collected below 400°C indicating that there are no long Mo–O bonds present in the system. This value decreases markedly above 400°C to 0.02, which is indicative of the presence of higher Mo–O

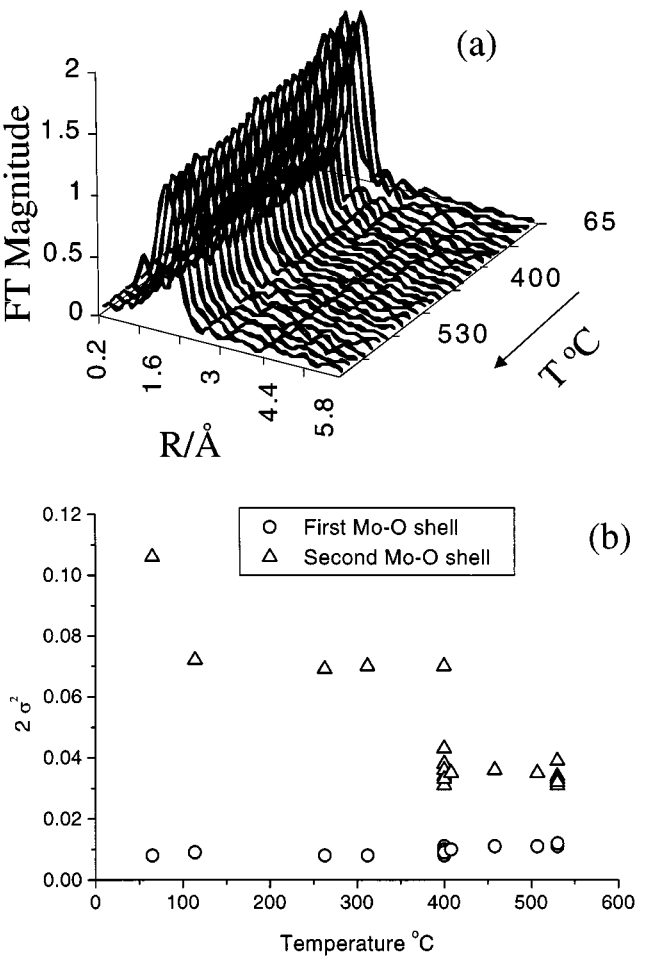

FIG. 8. (a) Stacked plot showing the Fourier transform magnitude of the Mo*K*-edge EXAFS data recorded during the course of heating the Bi_2MoO_6 precursor gel, in air. (b) Variation in Debye–Waller factor of the two Mo–O shells at ca. 1.78 and 2.2 Å (see text as well as Ref. (8) for details), as function of temperature.

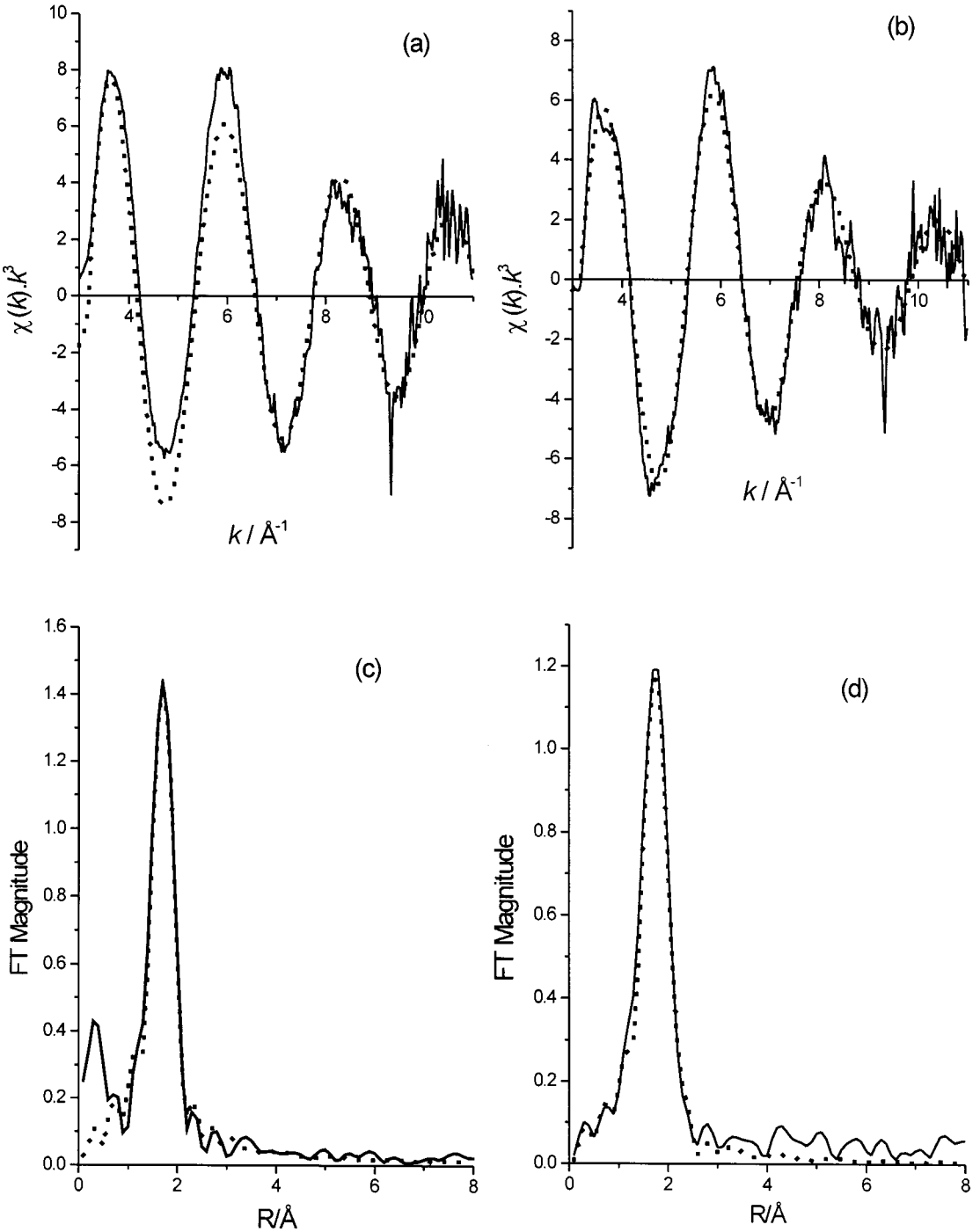

FIG. 9. Typical best fit to the EXAFS data of the starting material (at 50°C) and the final product (at 530°C), respectively. The solid line shows the experimental data and the dashed curve represents the best fit using the model described in Table 1.

distances. The value of σ^2 for the second shell continue to increase marginally above this temperature which is, once again, expected due to increase in thermal disorder. These results are consistent with the XANES data described earlier. Typical best fits to the experimental data are shown in Fig. 9. A tetrahedrally coordinated model fits very well for the data recorded at 50°C with a Mo–O bond length of 1.79 Å. For the 530°C data set, a distorted octahedral environment is the best model, as one would expect for a γ-phase, with four short Mo–O bonds at an average value of

TABLE 1
Structural Parameters Derived from Mo*K*-Edge EXAFS Data Recorded at Two Temperatures

	Atom-pair	Coordination number, N	Mo–O interatomic distance, R(Å)	$2\sigma^2$(Å^2)
50°C	Mo–O	4	1.75	0.009
	Mo–O	—	—	—
530°C	Mo–O	4	1.79	0.012
	Mo–O	2	2.23	0.023

1.8 Å, and two long Mo–O bonds at ca. 2.2 Å and these results are summarized in Table 1.

Finally, BiL_3-edge XAS data were also collected at temperatures similar to the one for molybdenum K-edge study. In Fig. 10 we show selected XANES data for the precursor and the one recorded at 530°C. There is only a small difference between the two scans indicating the Bismuth coordination environment did not change during phase formation which was also confirmed using the EXAFS data.

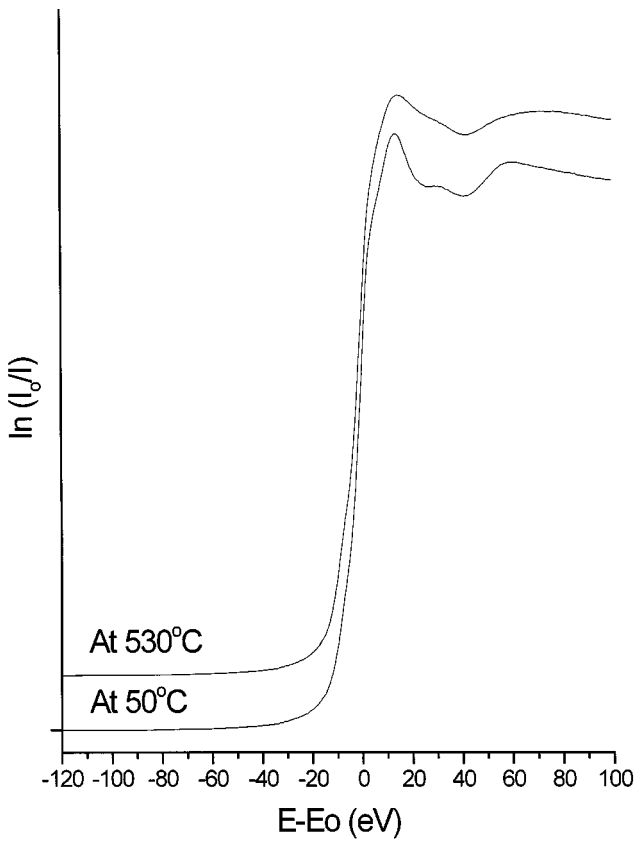

FIG. 10. BiL_{III}-edge XANES recorded at 50 and 530°C.

DISCUSSION

The TGA data show two weight losses, at 60°C and 250°C which is consistent with IR results that the first weight loss is due to the evaporation of physisorbed water and the second due to the complete loss of water and ammonia species from the system. The corresponding peaks are found in the DSC. In addition there are two other features at 131 and 171°C, which are not observed by the other techniques employed in this study. These two additional exotherms could be due to the rearrangement of the H bonds in the system. Although XRD of the dried precursor material show broad reflections indicative for the presence of the final Bi_2MoO_6-like phase, both XANES and EXAFS results clearly indicate that the octahedral coordination around molybdenum is formed only above 400°C. Although this coordination environment is consistent with the one suggested by Trifiro *et al.* (19), our XRD results clearly showed that there is no evidence for the formation of β phase prior to the production of γ phase. It is likely that first poorly ordered $Bi_2O_2^{2+}$ layers are formed at low temperatures and this may dominate the XRD data, since bismuth is a heavy scatterer of X rays. The XRD patterns shows sharp reflections for the material heated above 400°C. In addition, both XANES and EXAFS results show the formation of a distorted octahedral coordination around molybdenum above this temperature. Thus combining all these results it is clear that the Aurivilius structure of Bi_2MoO_6 are formed above 400°C.

This study also demonstrates the use of a multitechnique approach to understand the complex behavior of the formation of an active solid-state catalyst from a structurally ill-defined precursor gel.

ACKNOWLEDGMENTS

We thank EPSRC for financial support, CCLRC for the provision of beam time, and Daresbury laboratory for the use of ICSD data-base. L. M. Reilly thanks EPSRC and British Petroleum plc., U.K., for a CASE award. We also thank Professor Sir John Meurig Thomas, Dr. J. W. Couves, and Dr. J. F. C. Turner for useful discussions. Also we thank Dr. M. Odlyhya and Mr. G. Foster of the ULRIS thermal service for DSC and TGA measurements.

REFERENCES

1. R. K. Grasselli, J. D. Burrington, and J. F. Bradzil, *Faraday Disc.* **72,** 203 (1981).
2. R. K. Grasselli and J. D. Burrington, *Adv. Catal.* **30,** 133 (1981).
3. Y. Moro-Oka and W. Ueda, *Adv. Catal.* **40,** 233 (1994).
4. D. J. Buttrey, D. A. Jefferson, and J. M. Thomas, *Phil. Mag. A* **53,** 897 (1986).
5. R. G. Teller, J. F. Brazdil, and R. K. Grasselli, *Act. Crystallogr. Sect. C* **40,** 2001 (1984).
6. B. Aurivillius, *Ark. Kemi* **2,** 519 (1951).

7. M. R. Antonio, R. G. Teller, D. R. Sandstrom, M. Mehicic, and J. F. Bradzil, *J. Phys. Chem.* **92,** 2939 (1988).
8. G. Sankar, M. A. Roberts, J. M. Thomas, G. U. Kulkarni, N. Ranggavittal, and C. N. R. Rao, *J. Solid State Chem.* **119,** 210 (1995).
9. G. Sankar, P. A. Wright, S. Natarajan, J. M. Thomas, G. N. Greaves, A. J. Dent, B. R. Dobson, C. A. Ramsdale, and R. H. Jones, *J. Phys. Chem.* **97,** 9550 (1993).
10. G. Sankar and J. M. Thomas, *Top. Catal.* **8,** 1 (1999).
11. J. M. Thomas, G. N. Greaves, G. Sankar, P. A. Wright, J. Chen, A. J. Dent, and L. Marchese, *Angew. Chem. Intl.* **33,** 522 (1994).
12. B. S. Clausen, K. Graback, G. Steffensen, P. L. Hansen, and H. Topsoe, *Catal. Lett.* **20,** 23 (1993).
13. S. R. Davis, A. V. Chadwick, and J. D. Wright, *J. Phys. Chem.* **101,** 9901 (1997).
14. L. M. Colyer, G. N. Greaves, S. W. Carr, and K. K. Fox, *J. Phys. Chem.* **101,** 10105 (1997).
15. M. Oversluizen, W. Bras, G. N. Greaves, S. M. Clark, J. M. Thomas, G. Sankar, and B. Tiley, *Nucl. Inst. Meth. B* **97,** 184 (1995).
16. G. Nolze and W. Kraus, *J. Powder Diffr.* **13**, 256 (1998).
17. A. Corma, F. Rey, J. M. Thomas, G. Sanakar, G. N. Greaves, A. Cervilla, E. Llopis, and A. Ribeira, *Chem. Commun.* 1613 (1996).
18. K. Matsumoto, A. Kobayashi, and Y. Sasaki, *Bull. Chem. Soc. Jpn.* **48,** 1009 (1975).
19. F. Trifiro, H. Hoser, and R. D. Scarle, *J. Catal.* **25,** 12 (1972)